Journal of Materials Chemistry

Dynamic Article Links

Cite this: *J. Mater. Chem.*, 2012, **22**, 18902

www.rsc.org/materials

PAPER

Perovskite $Sr_{0.95}Ce_{0.05}CoO_{3-\delta}$ loaded with copper nanoparticles as a bifunctional catalyst for lithium-air batteries†

Wei Yang,[ab] Jason Salim,[c] Shuai Li,[ab] Chunwen Sun,*[ab] Liquan Chen,[ab] John B. Goodenough[d] and Youngsik Kim*[c]

Received 29th May 2012, Accepted 27th July 2012
DOI: 10.1039/c2jm33440b

$Sr_{0.95}Ce_{0.05}CoO_{3-\delta}$ (SCCO) particles loaded with copper nanoparticles on their surface are shown to be excellent, low-cost, and stable bifunctional catalysts for the oxygen-reduction and oxygen-evolution reactions (ORR and OER) in aqueous solution. Evidence for the presence of Ce^{3+} and Co^{2+} as well as Co^{4+} and Co^{3+} ions revealed by XPS measurements as well as XRD analysis indicates that a $CeCoO_{2.5}$ brownmillerite phase may be extruded to the surface. A surface Co^{4+}/Co^{3+} couple is known to be a good OER catalyst. The performance of the SCCO-based catalysts is better at higher current rates (>0.1 mA cm^{-2}) than that of Vulcan XC-72 and even close to that of the 50% Pt/carbon-black catalyst. This catalyst could be used in a metal/air battery or a PEM fuel cell as an efficient and stable bifunctional catalyst.

1. Introduction

A requirement for the proton-exchange-membrane (PEM) H_2/air fuel cell is an inexpensive, stable catalyst for the oxygen-reduction reaction (ORR) occurring at the cathode in an aqueous electrolyte. More challenging is the requirement for the Li/air rechargeable battery, *viz.* an inexpensive, stable bifunctional catalyst not only for the ORR, but also for the reverse oxygen-evolution reaction (OER). Moreover, the asymmetry of the ORR and OER introduces different discharge and charge voltages, which lower the efficiency of electrical-energy storage in a Li/air cell, and the rates of charge and discharge depend on the catalytic activities of the ORR and OER.

The concept of a Li/air battery with an organic electrolyte was introduced in 1996 by Abraham and Jiang.[1] Although it offered a theoretical specific energy density of 11 140 Wh kg^{-1} if oxygen is accessed directly from the air,[2] the discharge product Li_2O_2 is not stable in an organic electrolyte; on cycling, the Li_2O_2 gradually clogs the porous electrode to degrade the performance.[3,4] Moreover, the ORR and OER are both sluggish in an aprotic solution.[3,4] These observations indicate that an air electrode operates best in an aqueous electrolyte. The use of a lithium anode and an air cathode operating in an aqueous electrolyte is made possible by a solid Li-ion electrolyte acting as a separator of an organic liquid electrolyte (anolyte) on the lithium-anode side and an aqueous electrolyte (catholyte) on the air-cathode side.[5–10]

The cathode catalysts normally used to catalyze the air reactions are carbon black or carbon loaded with a noble metal.[1,9,11–13] Shao-Horn *et al.*[14] have used Pt–Au nanoparticles as a bifunctional catalyst to reduce the voltage gap between the ORR and OER to less than 0.8 eV at 50 mAh g^{-1} by using Au to enhance the ORR and Pt to lower the OER voltages. However, the carbon support of the costly noble-metal catalysts is thermodynamically unstable above 0.207 V *versus* the normal hydrogen electrode (NHE).[15,16] Oxidation of a carbon support, known as carbon corrosion, has been studied in PEM fuel cells; it decreases performance by accelerating the loss of active surface area,[17] altering pore morphology and surface characteristics,[18] either dropping noble-metal nanoparticles from the carbon-support surface or causing their aggregation into larger particles,[19,20] and changing the surface hydrophobicity which can cause gas-transport difficulties.[21] However, this issue has not yet attracted attention in the field of Li-air batteries.

Transition-metal oxides offer less costly alternative catalysts. The oxoperovskite cobaltates have been extensively studied as cathodes in solid oxide fuel cells operating in the temperature range 500–800 °C.[22] Also, Shao-Horn *et al.*,[23,24] have recently shown that transition-metal oxoperovskites containing surface cations with an e_g^1 electron configuration and good bulk

[a]*Beijing National Laboratory for Condensed Matter Physics, Institute of Physics, Chinese Academy of Sciences, Beijing 100190, China. E-mail: csun@iphy.ac.cn; Fax: +86-10-82649901; Tel: +86-10-82649901*
[b]*Key Laboratory for Renewable Energy, Chinese Academy of Sciences, Beijing Key Laboratory for New Energy Materials and Devices, Beijing 100190, China*
[c]*Richard G. Lugar Center for Renewable Energy, Department of Mechanical Engineering, Indiana University Purdue University, Indianapolis 46202, USA. E-mail: yk35@iupui.edu; Fax: +1-317-274-9744; Tel: +1-317-274-9711*
[d]*Texas Materials Institute, The University of Texas at Austin, Texas 78712, USA*

† Electronic supplementary information (ESI) available: XPS spectra of the $Sr_{0.95}Ce_{0.05}CoO_{3-\delta}$–Cu sample, discharge voltage profiles at different current densities of rechargeable lithium-air batteries with hybrid electrolytes and different catalysts. See DOI: 10.1039/c2jm33440b

electronic conductivity give a fast ORR and OER in alkaline solution. In this paper, we have chosen the perovskite $Sr_{0.95}Ce_{0.05}CoO_{3-\delta}$ (SCCO) to study the activities in aqueous solution in a Li/air rechargeable battery since intermediation-spin Co(III) ions on the surface of the cobaltates offer an e_g^1 configuration. James *et al.*[25] and Maignan *et al.*[26] studied structure and magnetism in the oxygen-deficient perovskites $Sr_{1-x}Ce_xCoO_{3-\delta}$ and found that the most metallic composition corresponds to $x = 0.05$ and $\delta \sim 0.28$.[26] Guo *et al.* studied the electrical properties of $SrCoO_{3-\delta}$ doped by CeO_2 and found that conductivity of $Sr_{1-x}Ce_xCoO_{3-\delta}$ was enhanced with increasing CeO_2 within the solubility limit. A conductivity over 500 S cm^{-1} was obtained at $x = 0.15$ when testing at 350–400 °C for the sample sintered at 1100 °C.[27] To the best of our knowledge, there is no report on the catalytic property of SCCO on ORR or OER so far. To further improve the catalytic performance of the SCCO, copper nanoparticles were deposited on the surface of the SCCO by the polyol method. A round-trip electric-energy storage efficiency of 75.2% with excellent long-term stability was observed in an aqueous Li/air cell.

2. Experimental section

2.1. Synthesis of perovskite $Sr_{0.95}Ce_{0.05}CoO_{3-\delta}$

In a typical sol–gel synthesis of SCCO, stoichiometric amounts of AR-grade strontium nitrate ($Sr(NO_3)_2$), cobalt nitrate ($Co(NO_3)_2 \cdot 6H_2O$), and cerium nitrate ($Ce(NO_3)_3 \cdot 6H_2O$) were dissolved in 110 ml of distilled water. Next, 8 ml of ethylene glycol (EG) and 2.31 g of citric acid were added to the above solution; a pink solution was obtained. After stirring the solution for 10 h at 80 °C on a hotplate, the solution became a stiff gel. The brown gel was dried in an electric oven at 250 °C to get a dark-gray precursor. Then the precursor was pelleted and sintered at 1100 °C in air for more than 72 hours by repeatedly grinding, pelleting, and sintering until no further reactions were detected.

2.2. Synthesis of perovskite $Sr_{0.95}Ce_{0.05}CoO_{3-\delta}$ loaded with copper nanoparticles

To load the copper nanoparticles on the SCCO sample, a reported poly process[28] was used. SCCO was first added to ethylene glycol (EG) while vigorously stirring it to form a suspension solution. Subsequently, $Cu(COOH)_2 \cdot H_2O$ dissolved in EG was added along with an EG solution of NaOH to adjust the pH of the solution to 10. Next, the liquid solution was refluxed at 197 °C for 1.5 hours. The suspension was separated by centrifugation and the precipitate was washed with water and alcohol three times before drying at room temperature. The copper loading was about 20 wt% analyzed by induced coupled plasma (ICP, Thermo Electron Corporation).

2.3. Characterization of materials

X-ray powder diffraction (XRD) patterns were recorded in a Philips XPert Pro diffractometer equipped with Cu Kα radiation over the 2θ range of 20° to 80° for each sample. Scanning electron microscopy (SEM) was performed on a scanning electron microscope (XL 30 S-FEG, FEI Co.). X-ray photoelectron spectroscopy (XPS) measurements were carried out with a spectrometer having Mg Kα radiation (ESCALAB 250, Thermofisher Co.). The binding energy was calibrated with the C 1s position of contaminant carbon in the vacuum chamber of the XPS instrument (284.8 eV).

2.4. Preparation of the anode and electrolyte

A lithium ribbon (99.9%) with a thickness of 0.38 mm was purchased from Sigma Aldrich, and disks with a diameter of 0.8 cm were cut for use as the anode. An organic non-aqueous liquid electrolyte, 1 M $LiPF_6$ in 1 : 1 (volume ratio) ethylene carbonate (EC) and diethyl carbonate (DEC), was purchased from Novolyte Corp. The Li-ion conducting glass ceramic (LiGC) plate, $Li_{1+x+y}Ti_{2-x}Al_xP_{3-y}Si_yO_{12}$, measuring 1 in. × 1 in. with a thickness of 150 μm and a Li-ion conductivity of 10^{-4} S cm^{-1}, was purchased from OHARA Inc. An aqueous liquid electrolyte of 0.01 M LiOH in pure DI water was prepared and used.

2.5. Preparation of the air catalytic electrode

The air catalytic electrode included a catalyst layer and a gas-diffusion layer. Teflon-treated carbon paper (Fuel Cell Store, Inc., 200 μm in thickness) was used as the gas diffusion layer. The carbon-supported electrocatalyst, Pt/C (50 wt% metal on carbon), was purchased from Alfa Aesar and used as received.

Catalyst ink solutions were prepared by mixing the catalyst (80 wt%) with ionomer (Tokuyama A4, 20 wt%) as a binder and ethanol (Decon Labs, Inc.) as a solvent in an ultrasonic bath for 1 h. The ink solution was sprayed onto one side of the Teflon-treated carbon paper. The area of the air electrode was 4 cm^2, and the mass loading of the catalyst layer was 1 mg cm^{-2} with a thickness of approximately 10 μm.

2.6. Assembly and testing of the Li-air battery

Fig. 1 shows a schematic illustration of the aqueous Li-air battery that was tested. The LiGC solid-electrolyte plate was first placed on top of the anode holder and sealed by epoxy. Next, the sealed anode holder and electrolyte plate were placed in an argon filled glove box where the water and oxygen concentrations were kept to less than 4 ppm. The Li metal disk and the organic liquid

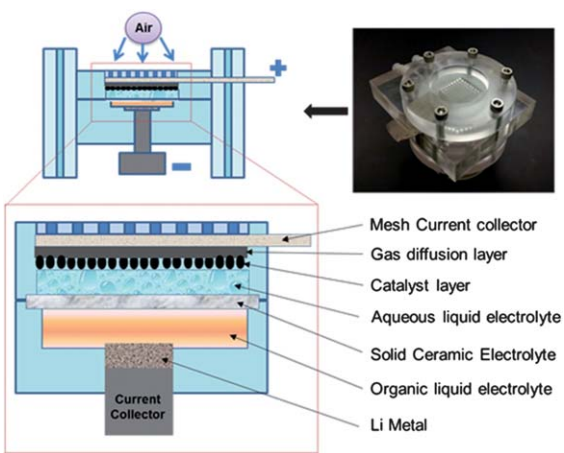

Fig. 1 Schematic diagram of a laboratory-sized aqueous Li-air battery.

electrolyte were loaded into the anode holder inside the glove box. After assembling the anode, the sealed assemblage was moved out of the glove box. The aqueous electrolyte was poured on top of the LiGC plate and then the air catalytic and diffusion layers were placed on the aqueous electrolyte. The assembled Li-air battery was exposed to ambient air and connected to the testing station. A Solartron 1470 cell tester was employed to perform the charge and discharge tests at a current density of 0.05 mA cm^{-2}.

3. Results and discussion

3.1. Physical characterization of the $Sr_{0.95}Ce_{0.05}CoO_{3-\delta}$–Cu catalyst

The phase purity and crystal structure of the products obtained were examined by XRD. Fig. 2 shows that the pattern of the obtained products can be indexed as a phase-pure tetragonal $Sr_{0.95}Ce_{0.05}CoO_{3-\delta}$, consistent with that of $SrCoO_{2.8}$ (JCPDS no. 39-1084). After depositing copper on the SCCO sample, the XRD pattern (curve b) clearly shows the peaks of cubic-phase metallic copper (JCPDS no. 04-0836) and of a small amount of Cu_2O phase. In addition, an un-indexed peak was observed around 25.2° in pattern b, indicating a new phase formed during the Cu deposition process. It is well known that perovskite $SrCoO_3$ and $LaCoO_3$ are easily reduced to brownmillerite-type vacancy-ordered phase $SrCoO_{2.5}$[29] and $LaCoO_{2.5}$[30,31] at low temperature, respectively. Therefore, the new phase may be $SrCoO_{2.5}$ or $CeCoO_{2.5}$.

The SEM images, Fig. 3, show the size and morphology of the SCCO particles and that copper nanoparticles with a size range of a few tens to several hundred nm are deposited on the surface of the SCCO particles.

X-ray photoelectron spectroscopy (XPS) was used to examine the composition of the SCCO sample and the valence state of the metal ions. A typical survey XPS spectrum for the SCCO–Cu sample indicates the existence of Sr, Ce, Co, Cu and O in the sample, as shown in Fig. S1a (see ESI).† The surface property of the copper nanoparticles was studied by XPS, as shown in Fig. 4a. The binding energy of the Cu $2p_{3/2}$ appears around 933.8 eV, indicating that CuO is absent. The peaks related to Cu and

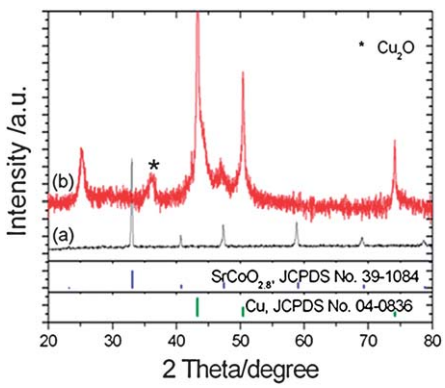

Fig. 2 XRD patterns of (a) $Sr_{0.95}Ce_{0.05}CoO_{3-\delta}$ and (b) $Sr_{0.95}Ce_{0.05}CoO_{3-\delta}$/Cu samples. The blue lines correspond to the peaks of the tetragonal phase $SrCoO_{2.8}$ (JCPDS no. 39-1084), and the green lines denote the peaks of cubic Cu phase (JCPDS no. 04-0836).

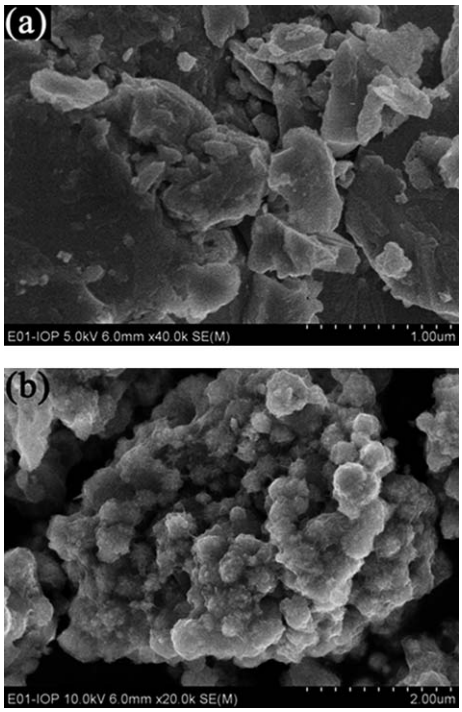

Fig. 3 Representative SEM images of the samples: (a) $Sr_{0.95}Ce_{0.05}CoO_{3-\delta}$, and (b) $Sr_{0.95}Ce_{0.05}CoO_{3-\delta}$–Cu.

Cu_2O are very close and differ by only 0.1 eV, but one can distinguish them from the positions of their LM2 auger transition in the XPS spectra, which are around 568 eV and 570 eV for Cu and Cu_2O, respectively.[32] There is no peak of Cu^{1+} around 570 eV in the CuLM2 auger spectrum (Fig. S1b)†, so the surface of the copper nanoparticles is mainly metallic Cu. The peaks around 780.8 eV and 796.6 eV shown in Fig. 4b can be assigned to Co^{3+} and Co^{4+}.[33,34] In addition, the formation of octahedrally coordinated high-spin Co^{2+} was also noted through the 2p satellite structure.[35,36] Fig. 4c shows the XPS spectrum of Ce3d; the bands v′ and u′ represent the satellites arising from the $Ce3d_{5/2}$ and $Ce3d_{3/2}$ ionization of Ce^{3+},[37,38] indicating that Ce is trivalent in SCCO. Since neither Ce^{3+} nor Co^{2+} would coexist with Co^{4+}, we are led to conclude that a brownmillerite $CeCoO_{2.5}$ phase has probably been extruded to the surface of the SCCO particles, which is consistent with the XRD analysis. Pinning of the Co^{4+}/Co^{3+} redox couple at the top of the O-2p bands of the $SrCoO_{3-\delta}$ phase with intermediate-spin Co^{3+} on the surface would catalyze the OER; the rate-limiting step of the ORR could be the displacement of an OH^- from a surface Co^{3+} ion by an absorbed O_2^- ion in the reaction, as shown in eqn (1), as discussed in ref. 23,24.

$$Co^{3+} - OH^- + O_2^-, \text{ads} \rightarrow Co^{4+} - O_2^{2-} + OH^- \quad (1)$$

3.2. Electrochemical properties of the $Sr_{0.95}Ce_{0.05}CoO_{3-\delta}$–Cu catalyst

In order to examine the possible application of $Sr_{0.9}Ce_{0.05}Co_{3-\delta}$–based materials in Li-air batteries and Li-air fuel cells, the

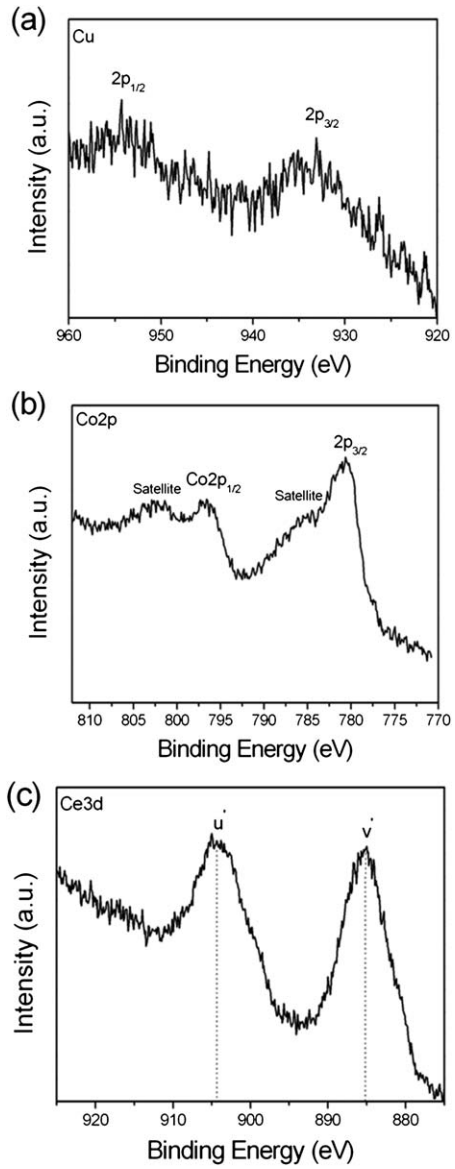

Fig. 4 XPS spectra of the $Sr_{0.95}Ce_{0.05}CoO_{3-\delta}$–Cu sample: (a) Cu 2p core level XPS spectrum, (b) Co 2p spectrum, and (c) Ce 3d spectrum.

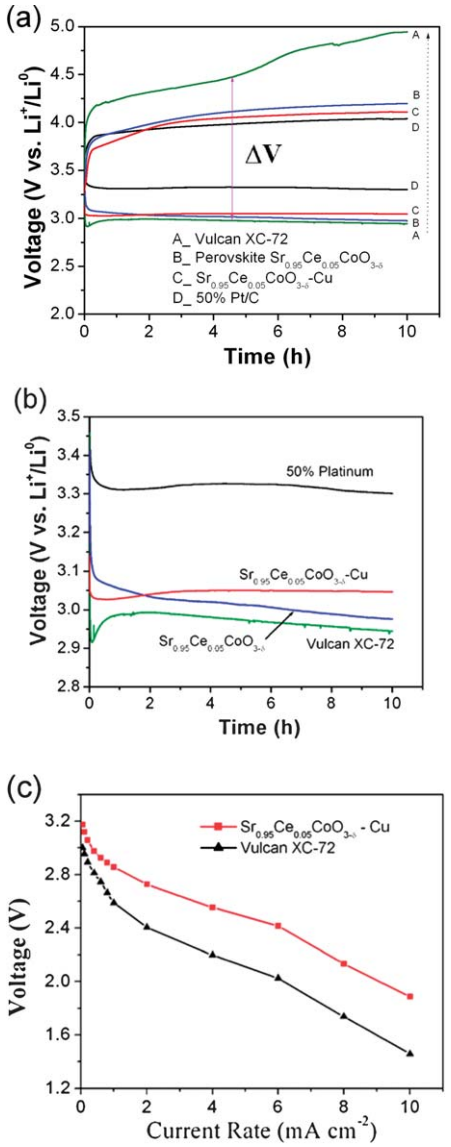

Fig. 5 (a) The first discharge–charge curves of the prepared lithium-air batteries with different catalysts, (b) magnified discharge curves to clearly show the difference among them in (a), and (c) comparison of discharge voltage as a function of current rates between Vulcan XC-72 and $Sr_{0.95}Ce_{0.05}CoO_{3-\delta}$–Cu catalysts.

catalysts were tested in a Li-air cell with hybrid electrolytes, as shown in Fig. 1. The first discharge and charge curves of cells with SCCO and SCCO loaded with Cu nanoparticles, respectively, were compared with those of cells with Vulcan XC-72 and state-of-the-art 50% Pt/carbon-black catalysts as shown in Fig. 5. The discharge and charge voltages of Li-air batteries are influenced greatly by the air electrode. The discharge voltages of the cells with SCCO and SCCO loaded with Cu nanoparticles, respectively, are lower than that of a 50% Pt/carbon-black catalyst, but slightly better than that of the Vulcan XC-72 at the rate of 0.05 mA cm^{-2}. However, at higher current rates (>0.1 mA cm^{-2}), the performance of the SCCO-based catalysts is clearly better than that of the Vulcan XC-72 (Fig. 5c and Fig. S2†). It is obvious that the charge voltages of cells with SCCO and SCCO loaded with Cu nanoparticles are much lower than that of the Vulcan XC-72 and even close to that of the 50% Pt/carbon-black catalyst. It should be noted that at the beginning of discharge for the Vulcan XC-72 catalyst, the operating voltage of the cell decreased quickly and then increased gradually and finally kept stable, which was not observed in the other three catalysts. This phenomenon can be ascribed to the electrode polarization.[7]

The differences between discharge and charge voltages (ΔV) as marked in Fig. 5a for the Vulcan XC-72, SCCO, SCCO–Cu, and 50%Pt/C catalysts are 1.51 V, 1.11 V, 0.98 V and 0.65 V, respectively. The round-trip efficiencies (the ratio of discharge to charge voltages) of the cells with SCCO and SCCO loaded with Cu nanoparticles as catalysts are 72.3% and 75.2%, respectively. These values are lower than that of the 50% Pt/carbon-black catalyst (83.0%), but much higher than that of the Vulcan XC-72 (58.8%). The SCCO catalysts loaded with Cu nanoparticles show

slightly better performance compared to the one without Cu. We believe that copper nanoparticles may play a dual role in this case. On the one hand, the copper nanoparticles improve the conductivity of the SCCO catalyst. On the other hand, the metallic copper could catalyze the electrochemical reduction of O_2 at its surface, starting from the copper corrosion in aqueous solution.[7] Generally, the copper corrosion in aqueous solution can be simply summarized as the following:[7,40,41]

$$2Cu + 1/2O_2 \rightarrow Cu_2O \quad (2)$$

If the Cu_2O formed on the copper surface obtains electrons from the external circuit, Cu_2O could be converted into fresh metallic copper according to eqn (3).[7,42]

$$Cu_2O + H_2O + 2e^{-1} \rightarrow 2Cu + 2OH^- \quad (3)$$

The overall reaction of eqn (2) and (3) is a typical O_2 electrochemical reduction on the copper surface, which can be expressed by eqn (4) as follows.

$$1/2O_2 + H_2O + 2e^{-1} \rightarrow 2OH^- \quad (4)$$

However, the Ce^{3+} ion of a surface $CeCoO_{2.5}$ phase may play a dominant role in the ORR, which needs further studies.

As for the charge–discharge mechanism of the Li/O_2 cell in an alkaline aqueous electrolyte, the chemical reaction is shown in eqn (5) below.[39]

$$4Li + O_2 + 2H_2O \leftrightarrow 4LiOH \quad (5)$$

The forward reaction represents the discharge process while the reverse one shows the charge process.

Fig. 6 shows the charge/discharge curves at a current density of 0.2 mA cm^{-2}. It clearly indicates that the cell can be reversibly charged/discharged and the SCCO–Cu catalyst has a good cycle performance. Fig. 7 shows the long-term discharge/charge curves of the prepared lithium-air batteries with the SCCO–Cu catalyst at a testing current density of 0.05 mA cm^{-2}. The test shows stable performance over 115 hours, which corresponds to

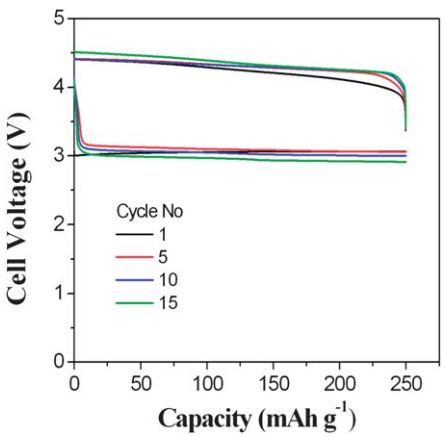

Fig. 6 The discharge–charge curves of the prepared lithium-air batteries with the SCCO–Cu catalyst at a current density of 0.2 mA cm^{-2} at different cycles.

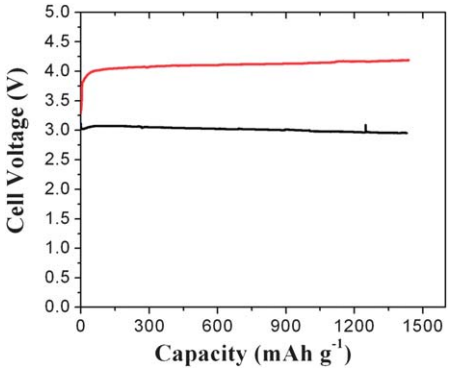

Fig. 7 Voltage *versus* discharge–charge capacity for the lithium-air batteries with the $Sr_{0.95}Ce_{0.05}CoO_{3-\delta}$–Cu catalyst.

1500 mAh g^{-1}. Considering the higher round-trip efficiency and excellent long-term stability as well as lower cost compared with noble metal catalysts, SCCO-based materials are a promising bifunctional catalyst for the Li-air battery, especially for the oxygen evolution reaction.

4. Conclusions

In summary, the SCCO–Cu composite has been synthesized and used as an air electrode in a Li–air cell with hybrid electrolytes. This novel catalyst exhibits an efficient and stable bifunctional catalytic activity. The improved performance of the SCCO–Cu catalyst can be ascribed to the synergetic effect of SCCO and copper. Indirect evidence for extrusion of a $CeCoO_{2.5}$ phase to the surface of the SCCO–Cu catalyst is consistent with a fast, stable OER on the $SrCoO_{3-\delta}$ phase; the relative roles of the Cu and the postulated $CeCoO_{2.5}$ surface phase on catalyzing the ORR await clarification. The preliminary results demonstrate the SCCO–Cu composite is a promising cathode material for the development of efficient, low cost, rechargeable metal-air batteries, Li-air fuel cells, and other rechargeable air-based energy storage devices.

Acknowledgements

This work is financially supported by the National Science Foundation of China (NSFC) (Grant no. 51172275), the National Key Basic Research Program of China (Grant no. 2012CB215402), and the Institute of Physics (IOP) start-up funding for the talents. Y. Kim's work is supported by Research Support Funds Grant (RSFG) at Indiana University Purdue University Indianapolis (IUPUI). John B. Goodenough thanks the Robert A. Welch Foundation of Houston, TX, for financial support.

Notes and references

1 K. M. Abraham and Z. Jiang, *J. Electrochem. Soc.*, 1996, **143**, 1.
2 B. Kumar, J. Kumar, R. Leese, J. P. Fellner, S. J. Rodrigues and K. M. Abraham, *J. Electrochem. Soc.*, 2010, **157**, A50.
3 A. Christensen, P. Albertus, R. S. Sanchez-Carrera, T. Lohmann, B. Kozinsky, R. Liedtke, J. Ahmed and A. Kojic, *J. Electrochem. Soc.*, 2012, **159**, R1.
4 G. Girishkumar, B. McCloskey, A. C. Luntz, S. Swanson and W. Wilcke, *J. Phys. Chem. Lett.*, 2010, **1**, 2193.

5 S. J. Visco, E. Nimon and B. D. Katz, *12th International Meeting on Lithium Batteries, Abstracts #397*, Nara, Japan, 2004.
6 Y. G. Wang and H. S. Zhou, *J. Power Sources*, 2010, **195**, 358.
7 Y. G. Wang and H. S. Zhou, *Chem. Commun.*, 2010, **46**, 6305.
8 Y. Lu, J. B. Goodenough and Y. Kim, *J. Am. Chem. Soc.*, 2011, **133**, 5756.
9 H. He, W. Niu, N. M. Asl, J. Salim, R. R. Chen and Y. Kim, *Electrochim. Acta*, 2012, **67**, 87.
10 L. Wang, X. Zhao, Y. Lu, M. Xu, D. Zhang, R. S. Ruoff, K. J. Stevenson and J. B. Goodenough, *J. Electrochem. Soc.*, 2011, **158**, A1379.
11 Y. C. Lu, D. G. Kwabi, K. P. C. Yao, J. R. Hardling, J. G. Zhou, L. Zuin and Y. Shao-Horn, *Energy Environ. Sci.*, 2011, **4**, 2999.
12 S. D. Beattie, D. M. Manolescu and S. L. Blair, *J. Electrochem. Soc.*, 2009, **156**, A44.
13 Y. C. Lu, H. A. Gasteiger and Y. Shao-Horn, *J. Am. Chem. Soc.*, 2011, **133**, 19048.
14 Y. Lu, Z. Xu, H. A. Gasteiger, S. Chen, K. Hamad-Schifferli and S. H. Yang, *J. Am. Chem. Soc.*, 2010, **132**, 12170.
15 M. Pourbaix, *Atlas of Electrochemical Equilibria in Aqueous Solutions*, Nat. Assoc. of Corrosion Engineers, Houston, Texas, 2nd edn, 1974, ch. IV, 17.1.
16 S. Maass, F. Finsterwalder, G. Frank, R. Hartmann and C. Merten, *J. Power Sources*, 2008, **176**, 444.
17 E. Antolini, *J. Mater. Sci.*, 2003, **38**, 2995.
18 K. H. Kangasniemi, D. A. Condit and T. D. Jarvi, *J. Electrochem. Soc.*, 2004, **151**, E125.
19 X. Wang, W. Li, Z. Chen, M. Waje and Y. Yan, *J. Power Sources*, 2006, **158**, 154.
20 Y. Shao, G. Yin, Y. Gao and P. Shi, *J. Electrochem. Soc.*, 2006, **153**, A1093.
21 R. Borup, J. Meyers, B. Pivovar, Y. S. Kim, R. Mukundan, N. Garland, D. Myers, M. Wilson, F. Garzon, D. Wood, P. Zelenay, K. More, K. Stroh, T. Zawodzinski, J. Boncella, J. E. McGrath, M. Inaba, K. Miyatake, M. Hori, K. Ota, Z. Ogumi, S. Miyata, A. Nishikata, Z. Siroma, Y. Uchimoto, K. Yasuda, K. I. Kimijima and N. Iwashita, *Chem. Rev.*, 2007, **107**, 3904.
22 C. W. Sun, R. Hui and J. Roller, *J. Solid State Electrochem.*, 2010, **14**, 1125.
23 J. Suntivich, H. A. Gasteiger, N. Yabuuchi, H. Nakanishi, J. B. Goodenough and Y. Shao-Horn, *Nat. Chem.*, 2011, **3**, 546.
24 J. Suntivich, K. J. May, H. A. Gasteiger, J. B. Goodenough and Y. Shao-Horn, *Science*, 2011, **334**, 1383.
25 M. James, K. S. Wallwork, R. L. Withers, D. J. Goossens, K. F. Wilson, J. Horvat, X. L. Wang and M. Colella, *Mater. Res. Bull.*, 2005, **40**, 1415.
26 A. Maignan, B. Raveau, S. Hébert, V. Pralong, V. Caignaert and D. Pelloquin, *J. Phys.: Condens. Matter*, 2006, **18**, 4305.
27 Q. T. Wei, R. S. Guo, F. H. Wang and H. L. Li, *J. Mater. Sci.*, 2005, **40**, 1317.
28 F. Fievet, J. P. Lagier, B. Blin, B. Beaudoin and M. Figlarz, *Solid State Ionics*, 1989, **32–33**, 198–205.
29 N. Ichikawa, M. Iwanowska, M. Kawai, C. Calers, W. Paulus and Y. Shimakawa, *Dalton Trans.*, 2012, DOI: 10.1039/c2dt30317e.
30 N. Orlovskaya, N. Browning and A. Nicholls, *Acta Mater.*, 2003, **51**, 5063–5071.
31 K. Vidyasagar, A. Reller, J. Gopalakrishnan and C. N. R. Rao, *J. Chem. Soc., Chem. Commun.*, 1985, 7–8.
32 T. Ghodselahi, M. A. Vesaghi, A. Shafiekhani, A. Baghizadeh and M. Lameii, *Appl. Surf. Sci.*, 2008, **255**, 2730.
33 B. W. Liu, Y. Zhang and L. Tang, *Int. J. Hydrogen Energy*, 2009, **34**, 435.
34 M. O'Connell, A. K. Norman, C. F. Hüttermann and M. A. Morris, *Catal. Today*, 1999, **47**, 123.
35 S. C. Petitto, E. M. Marsh, G. A. Carson and M. A. Langell, *J. Mol. Catal. A: Chem.*, 2008, **281**, 49–58.
36 L. Bi, H. Kim, G. F. Dionne and C. A. Ross, *New J. Phys.*, 2010, **12**, 043044.
37 C. Sun and L. Q. Chen, *Eur. J. Inorg. Chem.*, 2009, 3883.
38 D. K. Kim, K. Stöwe, F. Müller and W. F. Maier, *J. Catal.*, 2007, **247**, 101–111.
39 M. Song, S. Park, F. M. Alamgir, J. Cho and M. L. Liu, *Mater. Sci. Eng., R*, 2011, **72**, 203.
40 J. Kruger, *J. Electrochem. Soc.*, 1959, **106**, 847.
41 J. Kruger, *J. Electrochem. Soc.*, 1961, **108**, 503.
42 M. V. Vazquez, S. R. de Sanchez, E. J. Calvo and D. J. Schiffrin, *J. Electroanal. Chem.*, 1994, **374**, 179.